Inorganic Chemistry

Article

pubs.acs.org/IC

# New $Rh_2$(II,II) Architecture for the Catalytic Reduction of $H^+$

Travis A. White,[†] Suzanne E. Witt,[†] Zhanyong Li,[‡] Kim R. Dunbar,*[,‡] and Claudia Turro*[,†]

[†]Department of Chemistry and Biochemistry, The Ohio State University, Columbus, Ohio 43210, United States

[‡]Department of Chemistry, Texas A&M University, College Station, Texas 77843, United States

Supporting Information

**ABSTRACT:** Formamidinate-bridged $Rh_2^{II,II}$ complexes containing diimine ligands of the formula *cis*-$[Rh_2^{II,II}(\mu\text{-DTolF})_2(NN)_2]^{2+}$ (**$Rh_2$-$NN_2$**), where DTolF = *p*-ditolylformamidinate and NN = dppn (benzo[*i*]dipyrido[3,2-*a*:2′,3′-*h*]quinoxaline), dppz (dipyrido-[3,2-*a*:2′,3′-*c*]phenazine), and phen (1,10-phenanthroline), electrocatalytically reduce $H^+$ to $H_2$ in DMF solutions containing $CH_3COOH$ at a glassy carbon electrode. Cathodic scans in the absence of acid display a $Rh^{III,II/II,II}$ reduction at −0.90 V vs $Fc^+$/Fc followed by $NN^{0/-}$ reduction at −1.13, −1.36, and −1.65 V for **$Rh_2$-dppn$_2$**, **$Rh_2$-dppz$_2$**, and **$Rh_2$-phen$_2$**, respectively. Upon the addition of acid, **$Rh_2$-dppn$_2$** and **$Rh_2$-dppz$_2$** undergo reduction−protonation−reduction at each pyrazine-containing NN ligand prior to the $Rh_2^{II,II/II,I}$ reduction. The $Rh_2^{II,I}$ species is then protonated at one of the metal centers, resulting in the formation of the corresponding $Rh_2^{II,III}$-hydride. In the case of **$Rh_2$-phen$_2$**, the reduction of the phen ligand is followed by intramolecular electron transfer to the $Rh_2^{II,II}$ core in the presence of protons to form a $Rh_2^{II,III}$-hydride species. Further reduction and protonation at the $Rh_2$ core for all three complexes rapidly catalyzes $H_2$ formation with varied calculated turnover frequencies (TOF) and overpotential values ($\eta$): $2.6 \times 10^4$ $s^{-1}$ and 0.56 V for **$Rh_2$-dppn**, $2.8 \times 10^4$ $s^{-1}$ and 0.50 V for **$Rh_2$-dppz$_2$**, and $5.9 \times 10^4$ $s^{-1}$ and 0.64 V for **$Rh_2$-phen$_2$**. Bulk electrolysis confirmed $H_2$ formation, and further $CH_3COOH$ addition regenerates $H_2$ production, attesting to the robust nature of the architecture. The *cis*-$[Rh_2^{II,II}(\mu\text{-DTolF})_2(NN)_2]^{2+}$ architecture benefits by combining electron-rich formamidinate bridges, a redox-active $Rh_2^{II,II}$ core, and electron-accepting NN diimine ligands to allow for the electrocatalysis of $H^+$ substrate to $H_2$ fuel.

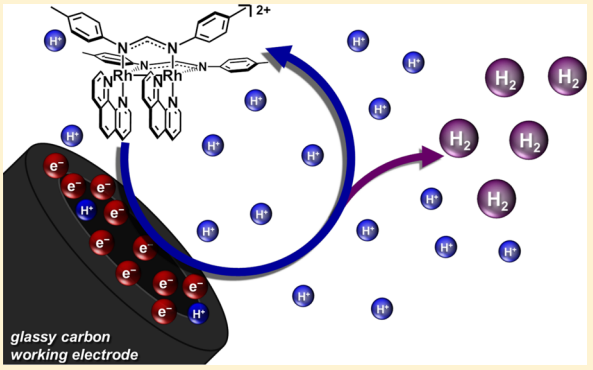


## INTRODUCTION

The generation of renewable, carbon-neutral fuels is critical for the future of the planet.[1,2] In particular, the catalytic production of $H_2$ and $O_2$ from $H_2O$ using sunlight is one attractive approach, thus storing solar energy in the form of chemical bonds.[3−5] Materials are available that couple the absorption of photons to the delivery of electrons at a given potential, making it possible for electrocatalytic processes to be easily driven by light.[4,5] Therefore, the development of highly active and stable molecular systems that are capable of efficient photo- or electrocatalytic reduction of $H_2O$ or $H^+$ to $H_2$ is greatly desired.[6−13] Utilizing homogeneous transition metal complexes for catalysis provides the benefit of facile tuning of the redox properties through the modification of the metal and/or ligand and also provides detailed insight into the electronic and structural requirements necessary to improve catalytic efficiency.

The presence of a second redox-active metal center in bimetallic architectures for catalytically driven reactions allows the molecular framework to better accommodate the addition and removal of redox equivalents as needed during the catalytic cycle, a feature that represents a potential advantage over monometallic systems. Dinuclear rhodium complexes bridged by carboxylate[14,15] or diphosphazane[16−20] functional groups have been reported to catalyze the conversion of $H_2O$ or hydrohalic acids (HX) into $H_2$. $Rh_2(\mu\text{-OAc})_4(H_2O)_2$ ($OAc^-$ = $CH_3COO^-$), *cis*-$[Rh_2(\mu\text{-OAc})_2(bpy)_2](OAc)_2$ (bpy = 2,2′-bipyridine), and *cis*-$[Rh_2(\mu\text{-OAc})_2(phen)_2](OAc)_2$ (phen = 1,10-phenanthroline) were shown to catalytically reduce $H^+$ in the presence of a $Ru^{II}$ or $Ir^{III}$ photosensitizer and a sacrificial donor following electron transfer to the $Rh_2^{II,II}$ scaffold.[14,15] In these systems, it is believed that the formation of a catalytically active $Rh_2^{II,I}$ or $Rh_2^{I,I}$ species is followed by axial protonation and subsequent $H_2$ evolution. Two-electron, mixed-valence, diphosphazane-bridged $Rh_2^{II,0}$ complexes $[Rh_2(\mu\text{-tfepma})_2L_2Cl_2]$ and $[Rh_2(\mu\text{-dfpma})_3X_2(L)]$ (tfepma = $CH_3N[P(OCH_2CF_3)_2]_2$; dfpma = $CH_3N(PF_2)_2$; $X^-$ = $Cl^-$, $Br^-$; L = CO, $PR_3$, CNR) function as single-component photocatalysts for HX conversion to $H_2$, whereby the dirhodium motif serves as both the photosensitizer and the catalytically active species.[16−20] Phosphine groups on the diphosphazane bridge are capable of accepting electrons from either the metal center or nitrogen lone pair, thereby facilitating multiple oxidation states of the rhodium metal centers.[17]

Tetraformamidinate-bridged $Rh_2^{II,II}$ compounds of the type $Rh_2(\mu\text{-form})_4$ (form = formamidinate ligand) are known to display photoinduced one-electron reduction of alkyl halides,

**Received:** August 10, 2015
**Published:** September 25, 2015





DOI: 10.1021/acs.inorgchem.5b01823
*Inorg. Chem.* 2015, 54, 10042−10048

RX, which generate $X^-$ and alkyl radicals, $R^\bullet$. This process was shown to occur via an outer sphere electron transfer from the excited state of the complex to RX, leading to the formation of the mixed-valent $Rh_2^{II,III}$ axially coordinated product $Rh_2(\mu\text{-form})_4\text{-X}$ and $R_2$.[21] Conversely, the electrochemical reduction of alkyl halides in the presence of the $Rh_2^{II,II}$ complexes $Rh_2(\mu\text{-form})_4$ results in axial $Rh_2(\mu\text{-form})_4\text{-R}$ complexes.[22−25] Coupled with their observed photochemical and electrochemical properties,[21,26,27] the relative ease of synthesis and air stability of these and related $Rh_2^{II,II}$ complexes represent attractive characteristics when compared to the two-electron, mixed-valence $Rh_2^{II,0}$ systems. $Rh_2(\mu\text{-form})_4$ complexes were previously shown to exhibit highly reducing $Rh_2(d\pi^*) \rightarrow Rh_2(d\sigma^*)$ excited states that can be accessed using broadband low-energy light ($\lambda_{abs}$ = 870 nm, $\varepsilon \sim 3000\ M^{-1}\ cm^{-1}$).[21] The low energy required for reactivity together with the accessibility of multiple metal oxidation states render $Rh_2(\mu\text{-form})_4$ complexes attractive candidates for photocatalytic applications, but limited solubility in polar solvents has precluded their widespread use. The substitution of two anionic bridging formamidinate ligands for two neutral bidentate chelating diimine ligands, NN, generates cationic complexes of the general formula $cis\text{-}[Rh_2^{II,II}(\mu\text{-form})_2(NN)_2]^{2+}$. These cationic compounds, which preserve the redox-active $Rh_2$(II,II) core, are significantly more soluble in polar solvents than the parent paddlewheel derivatives.[26,27]

The investigation of the electrocatalytic properties of $cis\text{-}[Rh_2^{II,II}(\mu\text{-form})_2(NN)_2]^{2+}$ compounds can provide crucial information regarding thermodynamic and kinetic requirements for catalysis as well as mechanistic insight into the catalytic processes.[28−34] Transition metal complexes that electrocatalytically reduce $H^+$ to $H_2$ have been investigated extensively and vary greatly with regard to turnover number (TON), turnover frequency (TOF), and overpotential ($\eta$).[9,11,35,36] To the best of our knowledge, the $cis\text{-}[Rh_2^{II,II}(\mu\text{-form})_2(NN)_2]^{2+}$ architecture has not been previously used for electrocatalytic reduction of $H^+$ to $H_2$. Herein, we report the electrocatalytic reduction of $H^+$ to $H_2$ by the series of complexes $cis\text{-}[Rh_2^{II,II}(\mu\text{-DTolF})_2(NN)_2]^{2+}$ (Figure 1), where

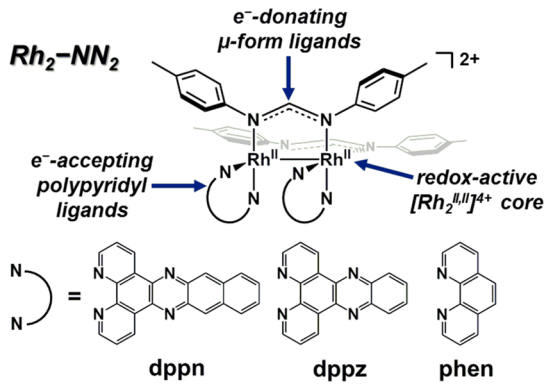


**Figure 1.** Schematic representation of the molecular structures of **$Rh_2$-dppn$_2$**, **$Rh_2$-dppz$_2$**, and **$Rh_2$-phen$_2$**.

DTolF = *p*-ditolylformamidinate and NN represents dppn (**$Rh_2$-dppn$_2$**, dppn = benzo[*i*]dipyrido[3,2-*a*:2′,3′-*h*]-quinoxaline), dppz (**$Rh_2$-dppz$_2$**, dppz = dipyrido[3,2-*a*:2′,3′-*c*]phenazine), and phen (**$Rh_2$-phen$_2$**, phen = 1,10-phenanthroline). The $Rh_2^{II,II}$ dimeric architecture possesses electron-donating formamidinate ligands, $\pi$-acceptor NN ligands, and two redox-active metal centers capable of modulating charge density throughout the catalytic cycle. By varying the NN ligand set, electronic requirements for electrocatalytic $H^+$ reduction can be ascertained. Coupling these properties with the availability of an open axial coordination site at each rhodium center for potential hydride bond formation affords highly active electrocatalysts for $H^+$ reduction.

## EXPERIMENTAL SECTION

**Materials.** All materials were used as received unless otherwise stated. $RhCl_3{\cdot}3H_2O$ was purchased from Pressure Chemical Company, and 1,10-phenanthroline (99%), 1,10-phenanthroline-5,6-dione (97%), *o*-phenylenediamine (99.5%), 2,4,6-trimethylphenol (97%), 1,5-cyclooctadiene (≥99%), sodium *tert*-butoxide (97%), silver tetrafluoroborate (98%), and *p*-toluidine (99%) were purchased from Aldrich Chemical Co.. Triethyl orthoformate (98%) was purchased from Sigma, and 2,3-naphthalenediamine (97%) was obtained from Spectrum Chemicals. Electrochemical grade tetrabutylammonium hexafluorophosphate (≥99.0%) was purchased from Fluka Analytical, recrystallized from EtOH, and stored in an 80 °C oven. *N*,*N*-Dimethylformamide (DMF), acetonitrile ($CH_3CN$), and glacial acetic acid ($CH_3COOH$) were obtained from Fisher Scientific. DMF was dried over 4 Å molecular sieves prior to use. $CH_3CN$ was distilled by refluxing over $CaH_2$ and stored under a $N_2$ atmosphere prior to use. $N_2$ (99.998%), Ar (99.998%), and $N_2/H_2$ mixture (95:5) were purchased from Praxair, Inc. (Danbury, CT, USA). Benzo[*i*]-dipyrido[3,2-*a*:2′,3′-*h*]quinoxaline (dppn),[37] (dipyrido[3,2-*a*:2′,3′-*c*]-phenazine (dppz),[38] $[cis\text{-}Rh_2^{II,II}(DTolF)_2(phen)_2](BF_4)_2$,[26] $[cis\text{-}Rh_2^{II,II}(DTolF)_2(dppz)_2](BF_4)_2$,[27] and $[cis\text{-}Rh_2^{II,II}(DTolF)_2(dppn)_2](BF_4)_2$[27] were prepared as previously reported.

**Methods and Instrumentation.** Electrochemical measurements were carried out under an inert atmosphere using a BASi model CV-50W voltammetric analyzer (Bioanalytical Systems, Inc.; West Lafayette, IN, USA). Cyclic voltammograms (CV) were obtained using a standard three-electrode configuration with a Pt wire auxiliary electrode, glassy carbon (3 mm diameter) working electrode, and a Ag/AgCl (3 M $NaCl_{aq}$) reference electrode in a glass tube capped with a vycor tip. Ferrocene (Fc) was added at the end of each set of cyclic voltammetry experiments, and potentials were referenced against the ferrocenium/ferrocene ($Fc^+/Fc$) couple (DMF, $E_{1/2}(Fc^+/Fc)$ = 0.55 V; $\Delta E_p$ = 90 mV). Typical CVs were recorded using the following conditions: 0.5 or 1.0 mM **$Rh_2$-NN$_2$** complex in DMF, 0.1 M $Bu_4NPF_6$ supporting electrolyte, 100 or 200 mV/s scan rate, and a $N_2$ atmosphere at 298 K.

Bulk electrolysis (BE) experiments were performed using a custom-built, airtight, two-compartment cell separated by a glass frit. A Pt wire auxiliary electrode was placed in the auxiliary compartment, which was filled with deoxygenated solvent. A Ag/AgCl (3 M NaCl(aq)) reference electrode ($E_{1/2}(Fc^+/Fc)$ = 0.55 V in DMF) and a high-density extruded graphite rod (Graphtek LLC; Buffalo Grove, IL, USA) working electrode were placed in the working compartment with a magnetic stir bar at the bottom. The reaction solution contained 0.5 mM **$Rh_2$-NN$_2$** and 20 mM $CH_3COOH$ in 5 mL of DMF (0.1 M $Bu_4NPF_6$ supp. electrolyte). The working and auxiliary compartments were deoxygenated for 20 min prior to applying a negative bias (−1.75 or −2.00 V vs $Fc^+/Fc$). A 100 $\mu$L aliquot of the 37 mL headspace was removed using a Hamilton gastight syringe and injected into a Shimadzu GC-2014 gas chromatograph (Ar carrier gas) with a packed 5 Å molecular sieves column (6 ft long × 1/8 in. o.d. × 2.1 mm i.d.) and a Shimadzu TCD-2014 thermal conductivity detector. The GC conditions were as follows: injector temp, 41 °C; column temperature, 30 °C; detector temperature, 150 °C; and gas flow, 25 mL/min.

## RESULTS AND DISCUSSION

**Electrochemical Properties.** The $cis\text{-}[Rh_2^{II,II}(\mu\text{-DTolF})_2(NN)_2]^{2+}$ molecular architecture displays multiple metal- and ligand-based redox couples, providing insight into the reactivity and energetics of the frontier molecular orbitals.


DOI: 10.1021/acs.inorgchem.5b01823
*Inorg. Chem.* 2015, 54, 10042−10048

Cyclic voltammograms of **$Rh_2$-dppn$_2$**, **$Rh_2$-dppz$_2$**, and **$Rh_2$-phen$_2$** measured in DMF are shown in Figure 2, and the

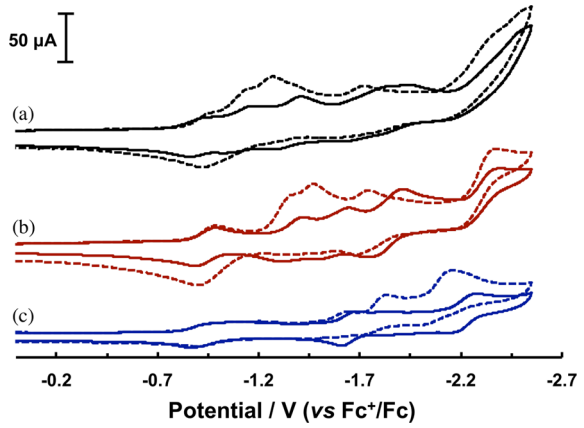


**Figure 2.** Cyclic voltammograms of 1.0 mM (a) **$Rh_2$-dppn$_2$**, (b) **$Rh_2$-dppz$_2$**, and (c) **$Rh_2$-phen$_2$** in the absence (solid line) and presence of 2 equiv of $CH_3COOH$ (dashed line) in DMF (0.1 M $Bu_4NPF_6$, 200 mV/s).

electrochemical processes, along with the corresponding redox potentials, are schematically depicted in Figure 3. Cathodic

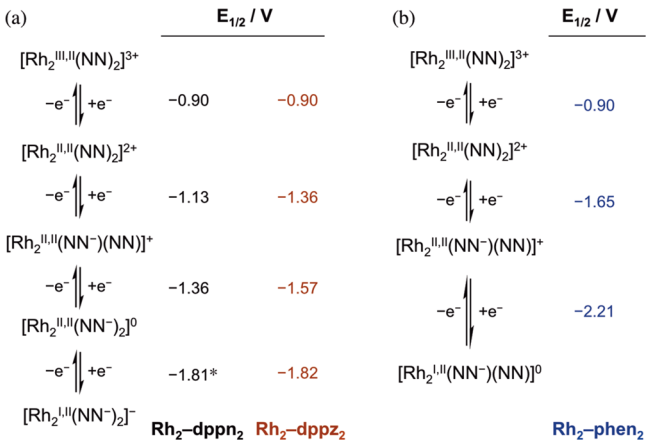


**Figure 3.** Electrochemical processes and the corresponding redox potentials for (a) **$Rh_2$-dppn$_2$** (black) and **$Rh_2$-dppz$_2$** (red) and (b) **$Rh_2$-phen$_2$** (blue); * denotes an $E_p^c$ value.

scanning reveals a $Rh_2^{III,II/II,II}$ reduction, $E_{1/2}([Rh_2\text{-}NN_2]^{3+/2+})$, at −0.90 V vs $Fc^+/Fc$ ($\Delta E_p$ = 90−100 mV) for all three complexes, as previously reported in $CH_3CN$.[27] The potential of the first one-electron diimine ligand-based reduction, $E_{1/2}([Rh_2\text{-}NN_2]^{2+/+})$, varies with NN identity and appears at −1.13, −1.36, and −1.65 V ($\Delta E_p$ = 80 mV) for **$Rh_2$-dppn$_2$**, **$Rh_2$-dppz$_2$**, and **$Rh_2$-phen$_2$**, respectively. $NN^{0/-}$ assignments were confirmed by measuring analogous Ru(II) systems, $[(bpy)_2Ru(NN)]^{2+}$ (NN = dppn, dppz, phen),[39,40] under our experimental conditions, whereby reversible $NN^{0/-}$ couples were observed at −1.14, −1.36, and −1.74 V, respectively (Figures S5−S7). Previous studies have shown that the molecular orbitals (MOs) of dppz can be described as a combination of isolated phenanthroline/quinoxaline MOs, therefore preventing extended aromaticity throughout the NN ligand set.[41−43] The same trend is expected for the dppn ligand, with the MO set possessing phenanthroline and benzoquinoxaline character. This ligand MO description explains how the $Rh_2^{III/II,II/II}$ couple occurs at the same potential throughout the NN = dppn, dppz, and phen series given that the electronic contribution from the proximal phen component dominates regardless of the identity of NN.

Further cathodic scanning reduces the second NN ligand, $E_{1/2}([Rh_2\text{-}NN_2]^{+/0})$, at −1.36 and −1.57 V for **$Rh_2$-dppn$_2$** and **$Rh_2$-dppz$_2$**, respectively. The small $\Delta E_{1/2}$ value of ∼200 mV between the first and second $NN^{0/-}$ couples in each complex indicates that the reduction occurs on two different NN ligands with some degree of electronic communication between them. The first and second reduction within the model complex $[Ru(bpy)_2(dppz)]^{2+}$ displays $\Delta E_{1/2}$ = 450 mV, in agreement with a previous report that the first two reductions occur on differing ligand $\pi^*$ systems (dppz and bpy).[44] The absence of the second $NN^{0/-}$ couple for **$Rh_2$-phen$_2$** implies strong electronic communication between the two phen ligands, shifting the second $phen^{0/-}$ wave to a more negative potential and outside the observable range under the present experimental conditions. The $Rh^{II,II/II,I}$ redox couple is observed at $E_p^c$ = −1.81 V, $E_{1/2}$ = −1.82 V ($E_p^c$ = −1.90 V, vide supra), and $E_{1/2}$ = −2.21 V for **$Rh_2$-dppn$_2$**, **$Rh_2$-dppz$_2$**, and **$Rh_2$-phen$_2$**, respectively.

The addition of $CH_3COOH$ ($pK_a$ = 13.5 in DMF)[45] does not alter the $E_{1/2}([Rh_2\text{-}NN_2]^{3+/2+})$ redox couple at −0.90 V for any of the measured complexes, indicating the lack of affinity for protons in the $Rh_2^{III,II}$ or $Rh_2^{II,II}$ oxidation states. However, further cathodic scanning of the **$Rh_2$-dppn$_2$** and **$Rh_2$-dppz$_2$** complexes results in an anodic shift and ∼2-fold current enhancement for both NN ligand-based redox couples (Figure 4a,b). The anodic shift from $E_p^c$ = −1.17 to −1.10 V ($[$**$Rh_2$-dppn$_2$**$]^{2+/+}$) and $E_p^c$ = −1.40 to −1.33 V ($[$**$Rh_2$-dppz$_2$**$]^{2+/+}$) is indicative of a proton-coupled electrochemical process attributed to $e^-/H^+$ addition at the dppn and dppz pyrazine subunit.[28] The corresponding ∼2-fold current enhancement suggests immediate reduction (overall ECE mechanism)[28,46,47] to form $dppnH^-$ and $dppzH^-$ moieties, respectively. This assignment was confirmed through the addition of $CH_3COOH$ aliquots to free dppn and dppz ligands, as well as to Ru(II) model systems. In all cases, a similar anodic shift coupled with ∼2-fold current enhancement was observed (Figures S2−S7). This proposed ECE mechanism for **$Rh_2$-dppn$_2$** and **$Rh_2$-dppz$_2$** is depicted in Figure 5. In contrast, no current enhancement was observed at the $phen^{0/-}$ redox couple for **$Rh_2$-phen$_2$**, only an anodic shift with increasing $CH_3COOH$ concentration ($E_p^c$ = −1.69 to −1.62 V) (Figure 4c). Given the lack of a pyrazine subunit within the phen ligand framework, no phen-based protonation is expected to occur using a weak acid source. The anodic shift is, therefore, proposed as $phen^{0/-}$ reduction increasing electron density at the formally $Rh_2^{II,II}$ core, allowing for protonation to be coupled with electron transfer from the $phen^-$ ligand to generate a $Rh_2^{II,III}$-hydride species.

The reduction of the dirhodium core to form a mixed-valent $Rh_2^{II,I}$ complex in both **$Rh_2$-dppn$_2$** and **$Rh_2$-dppz$_2$** is followed by protonation, generating a $Rh_2^{II,III}$-hydride at $E_p^c$ ∼ −1.70 V in the presence of low acid concentrations (up to 10 equiv $CH_3COOH$) (Figure 4a,b). The proposed $Rh^{III}$-hydride formation is similar to that reported by Savéant, whereby an electrochemically generated $Rh^I$ porphyrin is protonated by formic acid to form the corresponding $Rh^{III}$-hydride; the latter is then reduced to the $Rh^{II}$-hydride prior to catalysis.[48] The current responses at $E$ = −1.70 V for **$Rh_2$-dppn$_2$** and **$Rh_2$-dppz$_2$** in the presence of $CH_3COOH$ are slightly lower than those expected based on the current of the corresponding wave


DOI: 10.1021/acs.inorgchem.5b01823
Inorg. Chem. 2015, 54, 10042−10048

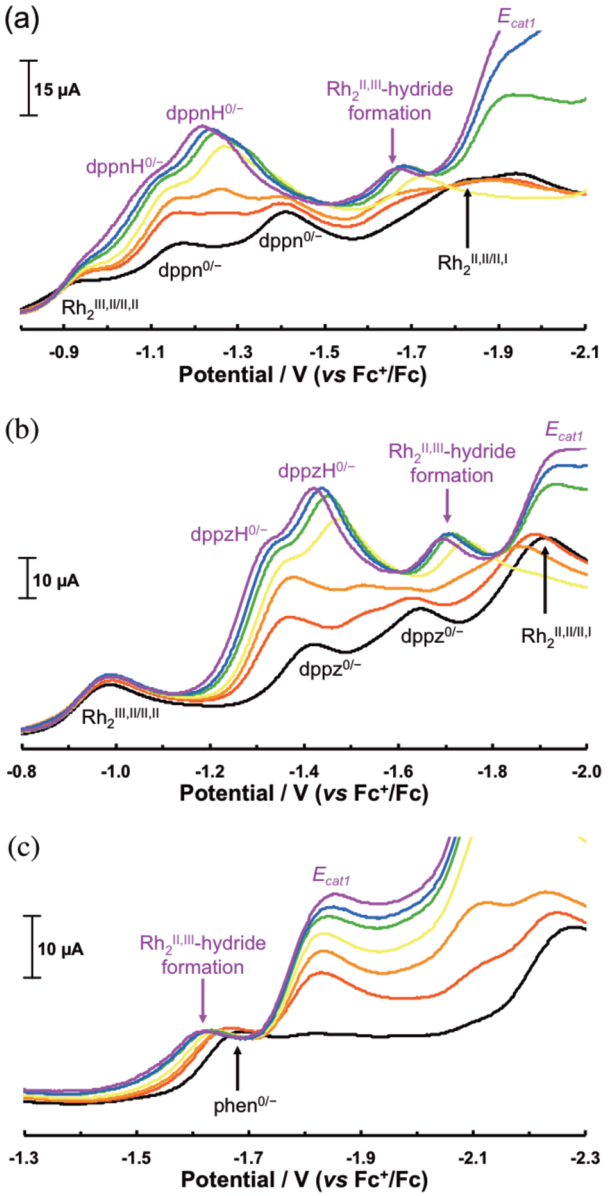


**Figure 4.** Cyclic voltammograms showing the forward cathodic scans of 1.0 mM (a) **$Rh_2$-dppn$_2$**, (b) **$Rh_2$-dppz$_2$**, and (c) **$Rh_2$-phen$_2$** in DMF (0.1 M $Bu_4NPF_6$, 200 mV/s) in the absence (black) and upon addition of $CH_3COOH$: 0.5 equiv (red), 1 equiv (orange), 2 equiv (yellow), 4 equiv (green), 6 equiv (blue), and 10 equiv (purple).

in the absence of acid; however, this decrease is not due to decomposition of the catalyst. The lower current can be attributed to the axial binding of acetate to the $Rh_2$ complexes, which effectively lowers the concentration of available $Rh_2$ catalyst for protonation. In fact, when sterically bulky 2,4,6-trimethylphenol was used as the proton source, the conjugate base of which is not able to coordinate to the axial position, no decrease in current is observed. For example, the cyclic voltammograms of **$Rh_2$-dppz$_2$** exhibit identical current values for the waves at $E_p^c$ = −1.75 V in the presence of 2,4,6-trimethylphenol (corresponding to the $Rh_2^{II,III}$-hydride formation) and for the $Rh_2^{II,II/II,I}$ couple at $E_p^c$ = −1.95 V in the absence of acid, indicating that the conjugate base plays an important role in electrocatalytic activity (Supporting Information). Increasing $CH_3COOH$ concentration results in further current enhancement at more negative potentials with

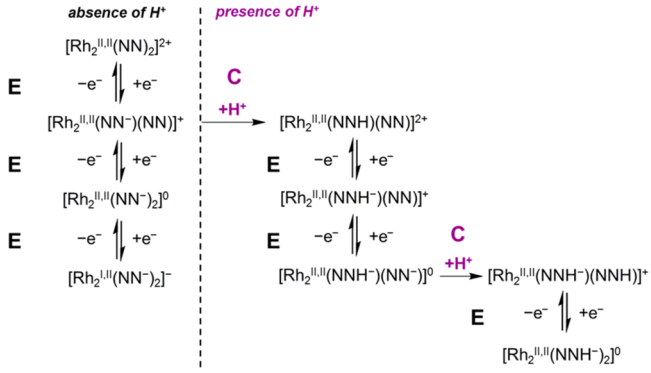


**Figure 5.** Electrochemical (E) and chemical (C) processes for **$Rh_2$-dppn$_2$** and **$Rh_2$-dppz$_2$** complexes involving the NN = dppn or dppz ligands in the absence and presence of $H^+$.

formation of new redox waves, suggesting that multiple mechanisms for $H^+$ reduction are present.

**Electrocatalytic Proton Reduction.** The ability of *cis*-$[Rh_2^{II,II}(\mu\text{-DTolF})_2(NN)_2]^{2+}$ complexes to electrocatalytically reduce $H^+$ to $H_2$ was examined using CV analyses through the comparison of the current response in the presence and absence of acid, $i_{cat}$ and $i_p$, respectively. At low acid concentrations, 0.5−20 equiv of $CH_3COOH$, two catalytic peak potentials are observed, $E_{cat1}$ and $E_{cat2}$. The first was measured at $E_{cat1}$ = −1.93 V for **$Rh_2$-dppn$_2$** and **$Rh_2$-dppz$_2$** and at −1.83 V for **$Rh_2$-phen$_2$**, whereas the second wave appears at $E_{cat2}$ = −2.20 V for all three complexes. Using **$Rh_2$-phen$_2$** as an example, the current response for the first catalytic wave ($i_{cat1}$) rapidly becomes independent of acid at [$CH_3COOH$] > 10 equiv, but the second wave ($i_{cat2}$) remains [$CH_3COOH$]-dependent at high acid concentrations (Figure 6). These results

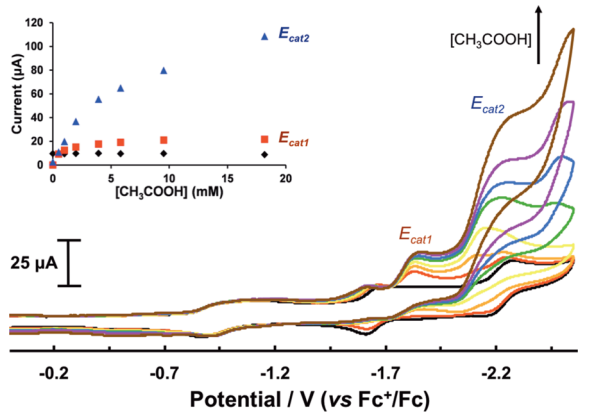


**Figure 6.** Cyclic voltammograms of 1.0 mM **$Rh_2$-phen$_2$** in the absence (black line) and presence of $CH_3COOH$ (0−18.2 mM) in DMF (0.1 M $Bu_4NPF_6$, 200 mV/s). Inset: Current response as a function of [$CH_3COOH$] measured at −1.65 (black diamonds), −1.85 (red squares), and −2.20 V (blue triangles).

are consistent with the presence of two competing catalytic processes, with a greater overall rate of catalysis for the second process as compared to that of the first, such that $k_{cat2} > k_{cat1}$.[46,49−51] Further increase in $CH_3COOH$, from 100 to 700 equiv (0.05−0.34 M), results in rapid catalytic current enhancement ($i_{cat2}/i_p$) at $E_{cat2}$ with a peak-shaped wave response indicative of local proton consumption competing with proton diffusion into the reaction-diffusion layer on the


DOI: 10.1021/acs.inorgchem.5b01823
*Inorg. Chem.* 2015, 54, 10042−10048

time scale of a CV scan (Figure 7).[32,33] Catalytic current enhancement values at $E_{cat2}$ become [$CH_3COOH$]-independent at concentrations ≥0.95 M (Figure 7, inset), as evidenced by the nonpositive slope.

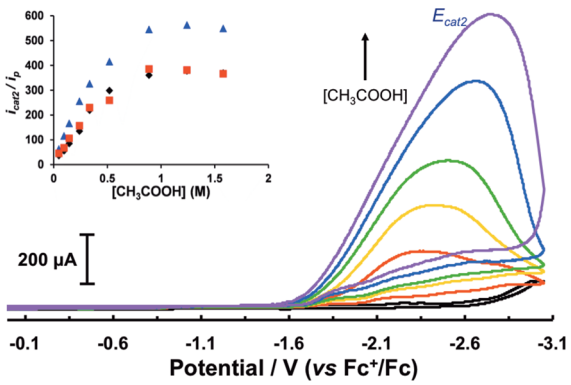


**Figure 7.** Cyclic voltammograms of 0.5 mM **$Rh_2$-phen$_2$** in the absence (black line) and presence of $CH_3COOH$ (0.05−0.34 M) in DMF (0.1 M $Bu_4NPF_6$, 100 mV/s) with the background current response from direct $CH_3COOH$ reduction at the bare glassy carbon electrode subtracted from each voltammogram. Inset: Catalytic current enhancement in the presence of acid ($i_{cat2}/i_p$) as a function of [$CH_3COOH$] at $E_{cat2}$ for **$Rh_2$-dppn$_2$** (black diamonds), **$Rh_2$-dppz$_2$** (red squares), and **$Rh_2$-phen$_2$** (blue triangles).

The [$CH_3COOH$]-independent regime provides a measure of the intrinsic catalytic function of **$Rh_2$-NN$_2$**, since the $i_{cat2}/i_p$ ratios can be used to calculate turnover frequencies (TOFs) according to eq 1

$$\frac{i_{cat}}{i_p} = 2.242\frac{n_{cat}}{n_p}\sqrt{\frac{RTk_{obs}}{n_pF\nu}} \quad (1)$$

where $n_{cat}$ is the number of electrons within the catalytic process (2 e$^-$), $n_p$ is the number of electrons for a noncatalytic redox process (1 e$^-$), $R$ is the ideal gas constant (8.314 V C K$^{-1}$ mol$^{-1}$), $T$ is temperature (298 K), $F$ is Faraday's constant (96 485 C mol$^{-1}$), $\nu$ is the scan rate (0.2 V s$^{-1}$), and $k_{obs}$ (∼ TOF) is the overall observed rate constant for catalytic turnover (s$^{-1}$).[29,31] The use of eq 1 results in TOF values of 2.6 × 10$^4$, 2.8 × 10$^4$, and 5.9 × 10$^4$ s$^{-1}$ for **$Rh_2$-dppn$_2$**, **$Rh_2$-dppz$_2$**, and **$Rh_2$-phen$_2$**, respectively. Overpotential ($\eta$) values of 0.56 (**$Rh_2$-dppn$_2$**), 0.50 (**$Rh_2$-dppz$_2$**), and 0.64 V (**$Rh_2$-phen$_2$**) were calculated by a method described by Fontecave and Artero using eq 2

$$\eta = |{E_{1/2}}^T - E_{cat2/2}| \quad (2)$$

where $E_{cat2/2}$ is the potential corresponding to half the current response ($i_{cat/2}$) of the catalytic wave and ${E_{1/2}}^T$ is the theoretical half-wave potential for $CH_3COOH$ in DMF.[45,52] The similar $\eta$ values are not surprising given that the redox-active molecular orbitals near the Rh metal center are primarily phen-based in all three complexes. However, the greater than 2-fold increase in TOF for **$Rh_2$-phen$_2$** compared to that for **$Rh_2$-dppn$_2$** and **$Rh_2$-dppz$_2$** suggests that the dppn and dppz ligands suppress catalysis to some degree, potentially due to NN ligand protonation consuming active substrate.

Constant potential electrolysis (CPE) of 0.5 mM **$Rh_2$-NN$_2$** and 20 mM $CH_3COOH$ at −1.75 and −2.00 V vs Fc$^+$/Fc confirmed the production of $H_2$ through the analysis of the reaction cell headspace using gas chromatography. A plot comparing $H_2$ production in the presence and absence of the **$Rh_2$-phen$_2$** catalyst electrolyzed at −1.75 V vs Fc$^+$/Fc (Figure S12) clearly indicates that the $Rh_2$ dimer is functioning as an electrocatalyst for $H^+$ reduction with a calculated turnover number (TON) of 5.5 after 1 h (Faradaic efficiency = 63% after 1 h). Following 24 h of electrolysis, additional $CH_3COOH$ was added to the reaction solution, and the initial rate of catalysis was regenerated (Figure S13). This observation attests to the robust nature of the **$Rh_2$-NN$_2$** architecture, indicating that the catalyst remains intact following exhaustive electrolysis. **$Rh_2$-dppn$_2$** and **$Rh_2$-dppz$_2$** were also electrolyzed in the presence of 20 mM $CH_3COOH$ at −1.75 V vs Fc$^+$/Fc and were found to inhibit catalysis. It is expected from the onset potential of $E_{cat1}$ shown in Figure 4 at low concentrations of $CH_3COOH$ that the mild applied potential of −1.75 V is not sufficient to rapidly drive catalysis. The low applied potential coupled with the protonation of the dppn and dppz ligands, which consume potentially active substrate, is expected to hinder catalysis. Applying a more negative bias of −2.00 V vs Fc$^+$/Fc initiates catalysis for **$Rh_2$-dppn$_2$** and **$Rh_2$-dppz$_2$** (Figure S14), coinciding with the observed catalytic current enhancement at $E_{cat1}$ in Figure 4.

To confirm that the **$Rh_2$-NN$_2$** architecture functions as a homogeneous catalyst, a rinse test of the electrode was performed (Figure S15).[53−55] A linear sweep voltammogram (LSV) was collected using **$Rh_2$-phen$_2$** in the presence of 20 equiv of $CH_3COOH$ scanning from −0.55 to −2.55 V vs Fc$^+$/Fc. The working electrode was then rinsed with DMF solvent and placed into a fresh DMF solution containing only 20 equiv of $CH_3COOH$ without polishing the electrode, and a cyclic voltammogram was collected over the same voltage range. The lack of a catalytic wave indicates that no surface-adsorbed, catalytically active species for proton reduction are present and that the **$Rh_2$-NN$_2$** architecture is a homogeneous catalyst.

Thorough data analysis provides insight into the mechanism of $H^+$ reduction by the **$Rh_2$-dppn$_2$**, **$Rh_2$-dppz$_2$**, and **$Rh_2$-phen$_2$** catalysts and is summarized in Figure 8. No current

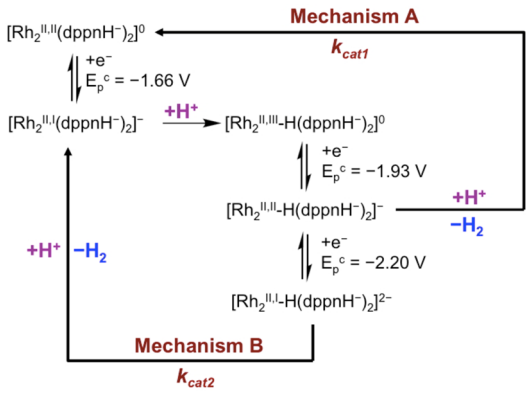


**Figure 8.** Proposed catalytic cycle for **$Rh_2$-dppn$_2$** depicting multiple pathways (mechanisms A and B) for $H^+$ reduction to $H_2$, whereby $k_{cat2} \gg k_{cat1}$. Potential values reported are vs Fc$^+$/Fc.

enhancement or anodic potential shift for the $Rh_2^{III,II/II,II}$ couple is observed in the presence of $CH_3COOH$, indicating insufficient nucleophilicity of the $Rh_2^{II,II}$ oxidation state to undergo protonation by weak acids. The complexes with diimine ligands containing pyrazine subunits, **$Rh_2$-dppn$_2$** and **$Rh_2$-dppz$_2$**, undergo reduction at pyrazine to form [$Rh_2^{II,II}$(NN$^-$)(NN)]$^+$, followed by ligand protonation and


DOI: 10.1021/acs.inorgchem.5b01823
Inorg. Chem. 2015, 54, 10042−10048

reduction to generate $[Rh_2^{II,II}(NNH^-)(NN)]^+$ via an ECE mechanism (Figure 5). The same process is observed for the second diimine ligand in **$Rh_2$-dppn$_2$** and **$Rh_2$-dppz$_2$**, whereby a second ECE mechanism affords the $[Rh_2^{II,II}(NNH^-)_2]^0$ species. **$Rh_2$-phen$_2$** does not possess a pyrazine subunit within the diimine ligand framework; therefore, reduction of the phenanthroline ligand ($[Rh_2^{II,II}(phen^{0/-})(phen)]^{2+/+}$, $E_{1/2}$ = −1.65 V) does not promote a ligand-based protonation. The shift of this wave to positive potential in the presence of $CH_3COOH$ is ascribed to protonation of the metal center with concurrent electron transfer from the phen$^-$ ligand to the dirhodium core such that the phen ligand coordinated to the redox-active $Rh_2^{II,II}$ core serves as an electron reservoir to enhance electron density at Rh and promote metal-hydride formation. Diimine- and dioxime-based ligand reductions to promote substrate interaction with a transition metal and eventual catalysis have been previously reported for $H^+$ and $CO_2$ reduction.[50,56−60]

When describing Rh-hydride formation for **$Rh_2$-dppn$_2$** and **$Rh_2$-dppz$_2$**, the spatially and electronically separated reduced pyrazine unit in each ligand and $Rh_2^{II,II}$ core limit influences of the ligands on the $Rh_2^{II,II/II,I}$ redox wave and subsequent metal protonation. In the absence of $CH_3COOH$, $Rh_2^{II,II/II,I}$ occurs at $E_p^c$ = −1.81 and −1.90 V for **$Rh_2$-dppn$_2$** and **$Rh_2$-dppz$_2$**, respectively. Upon $CH_3COOH$ addition, an anodic shift ($E_p^c$ = −1.66 and −1.70 V for **$Rh_2$-dppn$_2$** and **$Rh_2$-dppz$_2$**, respectively) for the corresponding wave is observed, consistent with the formation of a $Rh_2^{II,III}$-hydride via axial protonation at the $Rh_2^{II,I}$ center. The lack of further current enhancement at $E_p^c$ = −1.66 (**$Rh_2$-dppn$_2$**) and −1.70 V (**$Rh_2$-dppz$_2$**) indicates that the $Rh_2^{II,III}$-hydride species does not possess sufficient electron density at either the Rh metal center or hydride to undergo protonation. Reduction of the $Rh_2^{II,III}$-hydride to produce a $Rh_2^{II,II}$-hydride at $E_p^c$ = −1.93 V for both **$Rh_2$-dppn$_2$** and **$Rh_2$-dppz$_2$** and at $E_p^c$ = −1.83 V for **$Rh_2$-phen$_2$** possesses sufficient nucleophilic character to be protonated and evolve $H_2$. Interestingly, a second catalytic step is apparent at $E_{cat2}$ = −2.20 V, suggesting a competing pathway for $H^+$ reduction that observably dominates at greater $CH_3COOH$ concentrations. The intrinsic catalytic rate constant for catalysis occurring at $E_{cat2}$, $k_{cat2}$, is greater than that at $E_{cat1}$, $k_{cat1}$, given the rapid increase in catalytic current with greater [$CH_3COOH$] of the former. A similar observation was reported for a pentadentate $Co^{II}$-polypyridyl architecture, where competing $H^+$ reduction pathways are evident.[50] Mechanisms involving two or more different pathways for $H_2$ evolution in transition metals complexes are known throughout the literature.[48,49,61]

## CONCLUSIONS

Formamidinate-bridged, diimine-coordinated $Rh_2^{II,II}$ dimers function as electrocatalysts in the conversion of $H^+$ to $H_2$ with rapid TOF and relatively low $\eta$ values. The **$Rh_2$-phen$_2$** complex is able to rapidly produce $H_2$ without interference from ligand nitrogen atoms that can be protonated. The latter takes place in **$Rh_2$-dppn$_2$** and **$Rh_2$-dppz$_2$** and appears to hinder catalysis at low applied potentials and low $CH_3COOH$ concentrations due to substrate consumption by the ligand, but catalysis is reinstated with increasing $CH_3COOH$ concentration and/or a more negative applied bias. The key to $H^+$ reduction involves the protonation of the $Rh_2^{II,I}$ species to form a $Rh_2^{II,III}$-hydride intermediate that is further reduced and protonated to evolve $H_2$. Competing pathways exist at lower $CH_3COOH$ concentrations, as indicated by the presence of $E_{cat1}$ and $E_{cat2}$ catalytic waves. The *cis*-$[Rh_2^{II,II}(\mu\text{-form})_2(NN)_2]^{2+}$ architecture is an efficient electrocatalyst for $H_2$ production and, given the ability of these complexes to absorb visible light, makes them potentially useful as photocatalysts for $H^+$ reduction, a topic currently being investigated.

## ASSOCIATED CONTENT

### Supporting Information

The Supporting Information is available free of charge on the ACS Publications website at DOI: 10.1021/acs.inorgchem.5b01823.

DMF background CVs, free ligand CVs, $Ru^{II}$ model system CVs, **$Rh_2$-dppn$_2$** and **$Rh_2$-dppz$_2$** electrocatalytic CVs, bulk electrolysis data, rinse test CVs, graphs depicting overpotential, and explanation of calculations (PDF).

## AUTHOR INFORMATION


### Corresponding Authors

*(K.R.D.) E-mail: dunbar@mail.chem.tamu.edu.

*(C.T.) E-mail: turro.1@osu.edu.


### Notes

The authors declare no competing financial interest.

## ACKNOWLEDGMENTS

The authors wish to thank the U.S. Department of Energy, Office of Science, Office of Basic Energy Sciences (C.T., DE-SC0010542; K.R.D., DE-SC0010721) for financial support of this research.

## REFERENCES


(1) Lewis, N. S.; Nocera, D. G. *Proc. Natl. Acad. Sci. U. S. A.* **2006**, *103*, 15729.

(2) Balzani, V.; Credi, A.; Venturi, M. *ChemSusChem* **2008**, *1*, 26.

(3) Bard, A. J.; Fox, M. A. *Acc. Chem. Res.* **1995**, *28*, 141.

(4) Nocera, D. G. *Acc. Chem. Res.* **2012**, *45*, 767.

(5) Walter, M. G.; Warren, E. L.; McKone, J. R.; Boettcher, S. W.; Mi, Q.; Santori, E. A.; Lewis, N. S. *Chem. Rev.* **2010**, *110*, 6446.

(6) Frischmann, P. D.; Mahata, K.; Wurthner, F. *Chem. Soc. Rev.* **2013**, *42*, 1847.

(7) Han, Z.; Eisenberg, R. *Acc. Chem. Res.* **2014**, *47*, 2537.

(8) Inglis, J. L.; MacLean, B. J.; Pryce, M. T.; Vos, J. G. *Coord. Chem. Rev.* **2012**, *256*, 2571.

(9) McKone, J. R.; Marinescu, S. C.; Brunschwig, B. S.; Winkler, J. R.; Gray, H. B. *Chem. Sci.* **2014**, *5*, 865.

(10) Teets, T. S.; Nocera, D. G. *Chem. Commun.* **2011**, *47*, 9268.

(11) Wang, M.; Chen, L.; Sun, L. *Energy Environ. Sci.* **2012**, *5*, 6763.

(12) Du, P.; Eisenberg, R. *Energy Environ. Sci.* **2012**, *5*, 6012.

(13) Helm, M. L.; Stewart, M. P.; Bullock, R. M.; DuBois, M. R.; DuBois, D. L. *Science* **2011**, *333*, 863.

(14) Tanaka, S.; Masaoka, S.; Yamauchi, K.; Annaka, M.; Sakai, K. *Dalton Trans.* **2010**, *39*, 11218.

(15) Xie, J.; Li, C.; Zhou, Q.; Wang, W.; Hou, Y.; Zhang, B.; Wang, X. *Inorg. Chem.* **2012**, *51*, 6376.

(16) Elgrishi, N.; Teets, T. S.; Chambers, M. B.; Nocera, D. G. *Chem. Commun.* **2012**, *48*, 9474.

(17) Esswein, A. J.; Veige, A. S.; Nocera, D. G. *J. Am. Chem. Soc.* **2005**, *127*, 16641.

(18) Heyduk, A. F.; Nocera, D. G. *Science* **2001**, *293*, 1639.

(19) Powers, D. C.; Chambers, M. B.; Teets, T. S.; Elgrishi, N.; Anderson, B. L.; Nocera, D. G. *Chem. Sci.* **2013**, *4*, 2880.

(20) Powers, D. C.; Hwang, S. J.; Zheng, S.-L.; Nocera, D. G. *Inorg. Chem.* **2014**, *53*, 9122.

(21) Lutterman, D. A.; Degtyareva, N. N.; Johnston, D. H.; Gallucci, J. C.; Eglin, J. L.; Turro, C. *Inorg. Chem.* **2005**, *44*, 5388.




DOI: 10.1021/acs.inorgchem.5b01823
*Inorg. Chem.* 2015, 54, 10042−10048

(22) Bear, J. L.; Caemelbecke, E. V.; Ngubane, S.; Da-Riz, V.; Kadish, K. M. *Dalton Trans.* **2011**, *40*, 2486.
(23) Bear, J. L.; Yao, C. L.; Lifsey, R. S.; Korp, J. D.; Kadish, K. M. *Inorg. Chem.* **1991**, *30*, 336.
(24) Piraino, P.; Bruno, G.; Lo Schiavo, S.; Laschi, F.; Zanello, P. *Inorg. Chem.* **1987**, *26*, 2205.
(25) Ren, T.; Lin, C.; Valente, E. J.; Zubkowski, J. D. *Inorg. Chim. Acta* **2000**, *297*, 283.
(26) Chifotides, H. T.; Catalan, K. V.; Dunbar, K. R. *Inorg. Chem.* **2003**, *42*, 8739.
(27) Li, Z.; Leed, N. A.; Dickson-Karn, N. M.; Dunbar, K. R.; Turro, C. *Chem. Sci.* **2014**, *5*, 727.
(28) Bard, A. J.; Faulkner, L. R. *Electrochemical Methods: Fundamentals and Applications*, 2nd ed.; Wiley: New York, 2001.
(29) Nicholson, R. S.; Shain, I. *Anal. Chem.* **1964**, *36*, 706.
(30) Savéant, J.-M. *Chem. Rev.* **2008**, *108*, 2348.
(31) Saveant, J. M.; Vianello, E. *Electrochim. Acta* **1965**, *10*, 905.
(32) Rountree, E. S.; McCarthy, B. D.; Eisenhart, T. T.; Dempsey, J. L. *Inorg. Chem.* **2014**, *53*, 9983.
(33) Costentin, C.; Drouet, S.; Robert, M.; Savéant, J.-M. *J. Am. Chem. Soc.* **2012**, *134*, 11235.
(34) Costentin, C.; Passard, G.; Savéant, J.-M. *J. Am. Chem. Soc.* **2015**, *137*, 5461.
(35) Bullock, R. M.; Appel, A. M.; Helm, M. L. *Chem. Commun.* **2014**, *50*, 3125.
(36) Thoi, V. S.; Sun, Y.; Long, J. R.; Chang, C. J. *Chem. Soc. Rev.* **2013**, *42*, 2388.
(37) Foxon, S. P.; Green, C.; Walker, M. G.; Wragg, A.; Adams, H.; Weinstein, J. A.; Parker, S. C.; Meijer, A. J. H. M.; Thomas, J. A. *Inorg. Chem.* **2012**, *51*, 463.
(38) Greguric, A.; Greguric, I. D.; Hambley, T. W.; Aldrich-Wright, J. R.; Collins, J. G. *J. Chem. Soc., Dalton Trans.* **2002**, 849.
(39) Sun, Y.; Joyce, L. E.; Dickson, N. M.; Turro, C. *Chem. Commun.* **2010**, *46*, 2426.
(40) Vlcek, A. A.; Dodsworth, E. S.; Pietro, W. J.; Lever, A. B. P. *Inorg. Chem.* **1995**, *34*, 1906.
(41) Butsch, K.; Gust, R.; Klein, A.; Ott, I.; Romanski, M. *Dalton Trans.* **2010**, *39*, 4331.
(42) van der Salm, H.; Larsen, C. B.; McLay, J. R. W.; Fraser, M. G.; Lucas, N. T.; Gordon, K. C. *Dalton Trans.* **2014**, *43*, 17775.
(43) Fees, J.; Ketterle, M.; Klein, A.; Fiedler, J.; Kaim, W. *J. Chem. Soc., Dalton Trans.* **1999**, 2595.
(44) Fees, J.; Kaim, W.; Moscherosch, M.; Matheis, W.; Klima, J.; Krejcik, M.; Zalis, S. *Inorg. Chem.* **1993**, *32*, 166.
(45) Fourmond, V.; Jacques, P.-A.; Fontecave, M.; Artero, V. *Inorg. Chem.* **2010**, *49*, 10338.
(46) Canaguier, S.; Fourmond, V.; Perotto, C. U.; Fize, J.; Pecaut, J.; Fontecave, M.; Field, M. J.; Artero, V. *Chem. Commun.* **2013**, *49*, 5004.
(47) Kim, H. s.; Chung, T. D.; Kim, H. *J. Electroanal. Chem.* **2001**, *498*, 209.
(48) Grass, V.; Lexa, D.; Savéant, J.-M. *J. Am. Chem. Soc.* **1997**, *119*, 7526.
(49) Capon, J.-F.; Ezzaher, S.; Gloaguen, F.; Pétillon, F. Y.; Schollhammer, P.; Talarmin, J. *Chem. - Eur. J.* **2008**, *14*, 1954.
(50) Nippe, M.; Khnayzer, R. S.; Panetier, J. A.; Zee, D. Z.; Olaiya, B. S.; Head-Gordon, M.; Chang, C. J.; Castellano, F. N.; Long, J. R. *Chem. Sci.* **2013**, *4*, 3934.
(51) Roy, S.; Groy, T. L.; Jones, A. K. *Dalton Trans.* **2013**, *42*, 3843.
(52) Appel, A. M.; Helm, M. L. *ACS Catal.* **2013**, *4*, 630.
(53) Crabtree, R. H. *Chem. Rev.* **2015**, *115*, 127.
(54) Artero, V.; Fontecave, M. *Chem. Soc. Rev.* **2013**, *42*, 2338.
(55) Martin, D. J.; McCarthy, B. D.; Donley, C. L.; Dempsey, J. L. *Chem. Commun.* **2015**, *51*, 5290.
(56) Tong, L.; Zong, R.; Thummel, R. P. *J. Am. Chem. Soc.* **2014**, *136*, 4881.
(57) White, T. A.; Maji, S.; Ott, S. *Dalton Trans.* **2014**, *43*, 15028.
(58) Chen, Z.; Chen, C.; Weinberg, D. R.; Kang, P.; Concepcion, J. J.; Harrison, D. P.; Brookhart, M. S.; Meyer, T. J. *Chem. Commun.* **2011**, *47*, 12607.
(59) Machan, C. W.; Sampson, M. D.; Kubiak, C. P. *J. Am. Chem. Soc.* **2015**, *137*, 8564.
(60) Williams, O. M.; Cowley, A. H.; Rose, M. J. *Dalton Trans.* **2015**, *44*, 13017.
(61) Marinescu, S. C.; Winkler, J. R.; Gray, H. B. *Proc. Natl. Acad. Sci. U. S. A.* **2012**, *109*, 15127.


DOI: 10.1021/acs.inorgchem.5b01823
*Inorg. Chem.* 2015, 54, 10042−10048